nt Advances in Heat Transfer
B. Sundén and A. Žukauskas (Editors)

EXPERIMENTAL ANALYSIS OF FORCED CONVECTION HEAT TRANSFER IN A GROOVED CHANNEL

C. V. Herman, F. Mayinger
Lehrstuhl A für Thermodynamik, TU München
Arcisstraße 21, 8000 München 2, FRG.

ABSTRACT

This paper is concerned with heat transfer in forced convection in an asymmetrically heated flat plate channel with grooves located on the heated wall. The opposite plane wall is kept at ambient temperature. Both walls are maintained at uniform temperature. The working fluid is air. The thermal boundary layer develops along the test section under laminar flow conditions. The aspect ratio of the grooves, w/h, is 4 : 1 and the ratio of channel width to groove depth is 2 : 1. Experiments were performed for different Reynolds numbers. Temperature fields and local Nusselt numbers were measured by means of holographic interferometry. In the paper, the visualized temperature fields are analysed and the temperature distributions are discussed. The distribution of the local Nusselt number is presented for different Reynolds numbers. Average Nusselt numbers for groove-channel periods along the channel are evaluated and the influence of the grooves on the heat transfer process is investigated.

Introduction

In order to improve the thermal performance of heat transfer devices, different techniques of heat transfer augmentation are implemented in the design of heat transfer surfaces [1, 2]. In this study, the basic geometry, a parallel plate channel, has been modified by introducing transversal grooves, in order to periodically interrupt the plane heat transfer surface.

The investigated geometry and the physical situation are presented schematically in Fig. 1. Heat transfer is analyzed experimentally ([3, 4]) in a parallel plate channel with four transversal grooves on the heated wall. The grooves and the channel regions between the grooves are w = 0.02 m long, the depth of the grooves is h = 0.005 m, corresponding

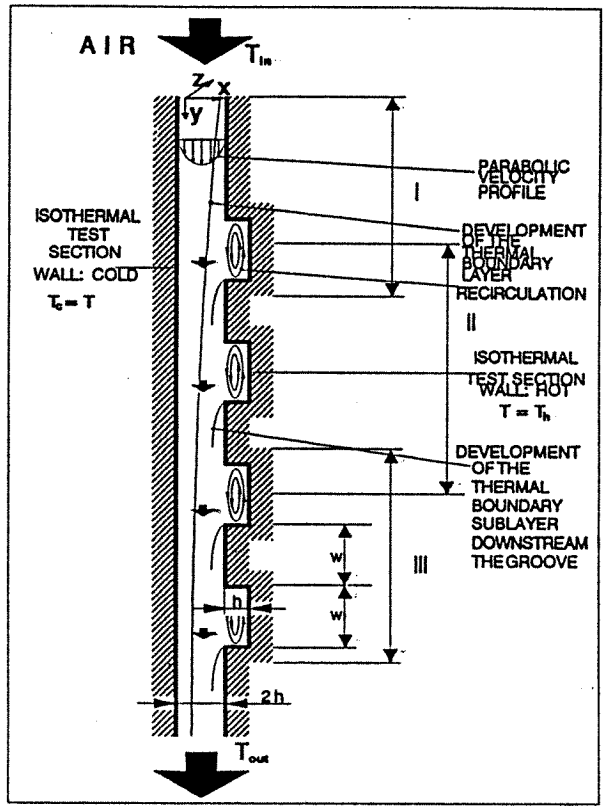

Fig. 1 Schematic of the investigated geometry and the physical situation

to one half of the channel height. The walls of the test section are maintained at uniform but different temperatures. The flow is fully developed with parabolic velocity profiles at the entrance of the test section. The thermal boundary layer develops along the heated wall of the test section and the influence of the grooves on the heat transfer process is investigated. The two-dimensional temperature fields were visualized and reconstructed using holographic interferometry, and local and average heat transfer data were obtained.

A geometry with grooves (or ribs) is frequently encountered in various engineering applications like the cooling of reactor cores, biomedical applications, design of various heat exchangers, cooling of electronic equipment, and so on. Heat transfer in the basic geometry — parallel plate channels, rectangular and circular ducts — was reviewed and

treated in detail in the literature [5]. Of practical interest is the experimental work of Aung [6], who analysed heat transfer on a single cavity and the influence of the aspect ratio of the cavity on the heat transfer by means of interferometry. The temperature profiles that he obtained, as well as the local heat transfer coefficients, show similar behaviour as in the present analysis. Heat transfer and fluid flow in a periodically grooved geometry for fully developed flow and periodically repeating thermal conditions were treated in [7-9]. Especially possibilities of resonant heat transfer enhancement were analysed, and the experimental results confirmed the numerical predictions [10]. Trollheden and Sundén [11] numerically investigated laminar flow in a symmetrically heated parallel plate channel with large cavities, a geometry similar to the one treated in this paper. The walls of the channel were maintained at uniform temperature. The flow field was fully developed with periodically repeating cycles and thermally fully developed regime — contrasted to the thermally developing situation analysed in this paper. They have found that moderate heat transfer augmentation was achieved with high pressure drop penalty in comparison with values for a straight duct. Sundén and Trollheden [12] investigated the same geometry with uniform heat flux imposed at the channel walls, and they found a decrease in heat transfer compared to the flat plate channel. Lockett and Collins [13] investigated heat transfer in turbulent flow over square and rounded rib-roughness elements using holographic interferometry. Heating was provided by electrical pad resistance heaters. The authors were faced with severe refraction and beam crossing effects in the interferometric investigation in some parts of the near wall region. These were overcome by extrapolation to the wall, so that local surface heat transfer data could be obtained. In the present study, accurate evaluation of local heat transfer coefficients was possible, as by the appropriate selection of the spanwise dimension of the test section and of the location of the focusing plane, no beam crossing effects were encountered, so that the parabolic approximation allowed for the reconstruction of temperature fields with sufficient accuracy. The local heat transfer distribution in the geometry investigated in [13] shows similar behaviour as in this investigation.

Experimental Apparatus

The experimental apparatus used in the heat transfer measurements and in the visualization of temperature fields is shown in Fig. 2. The experimental channel is in the vertical position and it consists of the entry section, the test section and the exit section. The entry section is 0.9 m long (y direction), $2h = 0.01$ m high (x direction) and $d = 0.22$ m wide (z direction, corresponds to the direction and length of transillumination by laser light) rectangular duct. The selected length of the entry section provides the fully developed velocity profiles at the entrance of the test section. The width to height ratio (22 : 1) is needed to obtain the essentially two dimensional temperature distribution, significant for an accurate reconstruction of temperature fields from interferograms, as the method of holographic interferometry is characterized by averaging in the spanwise (transillumination) direction. The test section is 0.22 m long and both its walls, made of aluminium, are provided with water channels. Circulating water from two constant temperature water baths, in three parallel loops for each channel wall, maintains wall temperatures constant providing isothermal boundary conditions. The plane cold wall is kept at ambient temperature and the grooved wall is heated to a temperature which is $\overline{\Delta T}$ above the value for the cold wall. Glass windows allow for the transillumination of the investigated region. The exit section is 0.3 m long, so that it removes possible downstream effects from the test

section, and it carries the blower creating the air flow. The blower is operating in a suction mode, and the flow velocity is varied by varying the Dc supply voltage of the blower.

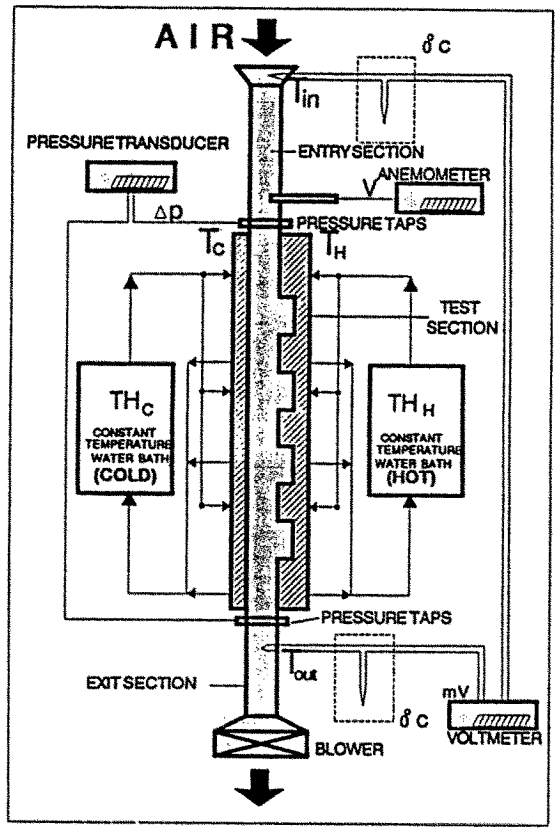

Fig. 2 Schematic of the experimental apparatus

Air inlet and outlet temperatures were measured by two batteries of nickelchrom-constantan thermocouples at locations as indicated in Fig. 2. Flow velocity profile measurements were taken by a Schiltknecht hot wire anemometer thermo air type 442 calibrated by a rotameter. In the pressure drop measurements, a pressure transducer Setra Series 239 calibrated by a Betz manometer was used. The pressure transducer was connected to the four pressure taps in the flange between the entry and test sections and in the flange between the test section and the exit section. The temperatures of the hot wall and of the cold wall were monitored by 25 nickelchrom-constantan thermocouples providing reference values for the interferometric measurements.

Measuring Technique

The method of holographic interferometry is widely accepted in the study of transport phenomena [14-17] and it was used in the visualization of temperature fields in the experiments described in this paper. Being a non-invasive method, it is well suited for measurements in complex geometries. Thus qualitative information on the temperature fields and — by evaluating the interferograms — also quantitative heat transfer data was obtained without disturbing the investigated physical process.

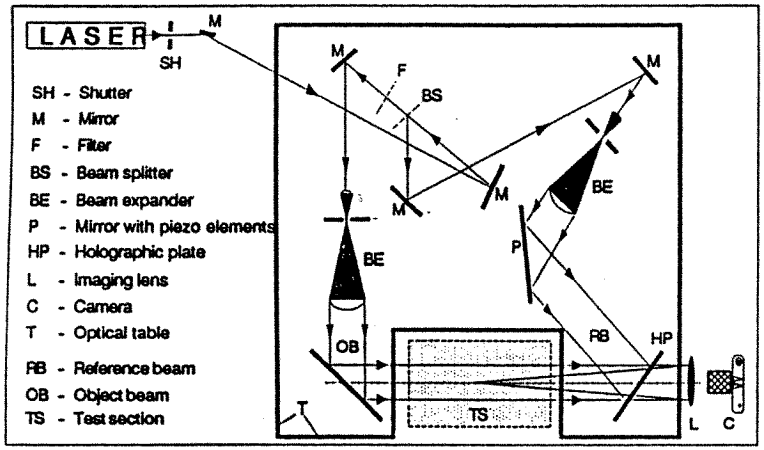

Fig. 3 Schematic of the optical setup for holographic interferometry

The optical setup used in the measurements (Fig. 3) corresponds to the basic optical arrangement discussed in [14 and 15]. The procedure of the reconstruction of temperature profiles from interferograms is described in [17]. In the experiments, an Argon ionen laser with $\lambda = 514.5$ nm wavelength and 0.5 m coherence length served as light source. The interferograms were recorded using the real time method (further details are given in [3 and 4]) on photographic film, and the processed negatives were then analysed and measured by a photometer. Since the test section is longer (0.22 m) than the diameter of the expanded laser beam (0.078 m), temperature fields were recorded at three different heights of the test section (indicated by I, II and III in Fig. 1) in different experimental runs.

Discussion of Results

Experimental Parameters

The thermal boundary conditions in heat transfer measurements in the grooved geometry are isothermal (T_H for the heated wall and T_C for the plane wall at T_{in}). The average temperature difference between hot and cold wall $\overline{\Delta T}$ was evaluated by taking average values of thermocouple readings, and it was maintained constant in the visualization experiments at different test section heights. The results discussed in this paper were obtained for $\overline{\Delta T} \approx 43$ K. Interferograms were recorded also for $\overline{\Delta T} \approx 30$ K and $\overline{\Delta T}$

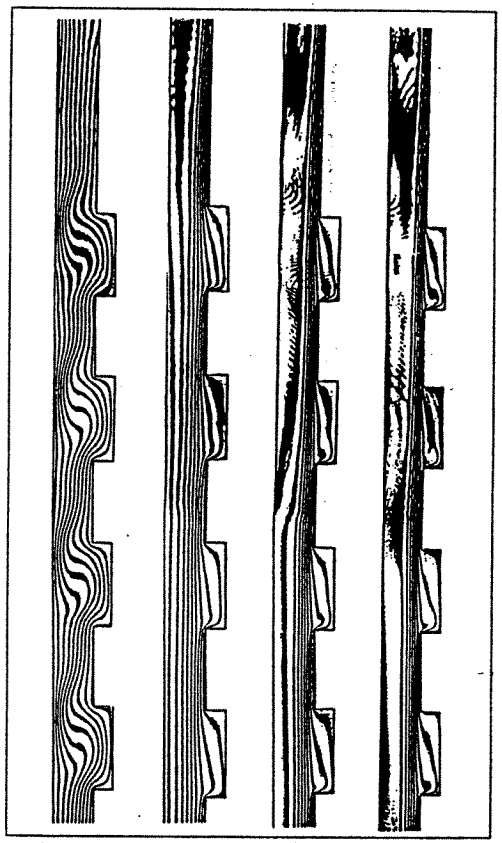

Fig. 4 Typical interferogram sets for $v_m = 0$ m/s, Re = 354, Re = 519 and Re = 1760 (from left to the right, respectively) recorded using the infinite fringe field arrangement. The average temperature difference between the hot and the cold wall is $\overline{\Delta T} \approx 30$ K. Fringes correspond to isotherms with ΔT/fringe pair ≈ 3 K. Air flows from top to bottom in the field of view.

60 K, and for the three temperature differences the same basic behaviour was observed. Experimental runs were performed for Reynolds numbers in the range of $290 \leq Re \leq 2000$. The Reynolds number was based on the hydraulic diameter D_h as the characteristic length,

$$Re = v_m D_h / \nu. \tag{1}$$

From the measured velocity profiles, the average flow velocity across the channel v_m was evaluated with an estimated uncertainity of 7%.

Temperature fields

A set of visualized temperature fields for $\overline{\Delta T} \approx 30$ K for $v_m = 0$ m/s and three different Reynolds numbers obtained by using the infinite fringe field technique is presented in Fig. 4, and it is a typical representative of the thermal behaviour of the system. The four pictures are obtained by assembling interferograms recorded at the three different heights (I, II and III in Fig. 1), and the temperature distributions originating from the different experimental runs show very good agreement.

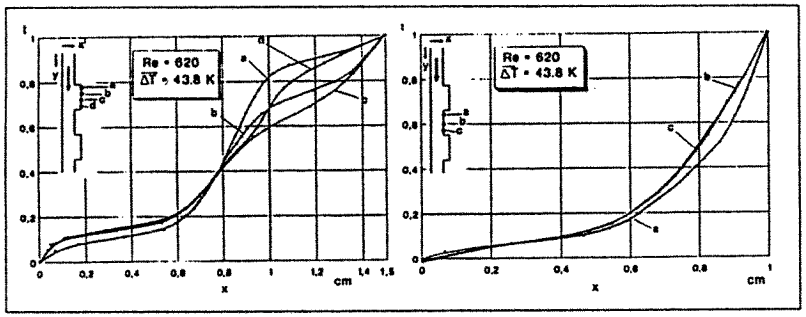

Fig. 5 Typical reconstructed temperature profiles at cross sections a) y = 5.17 cm, b) y = 6.13 cm, c) y = 6.83 cm and d) y = 6.96 cm in the region of the first groove (diagram left) and at cross sections a) y = 7.04 cm, b) y = 7.87 cm and c) y = 8.88 cm between the first groove and the second groove (diagram right) for Re = 620 and $\overline{\Delta T}$ = 43.8 K.

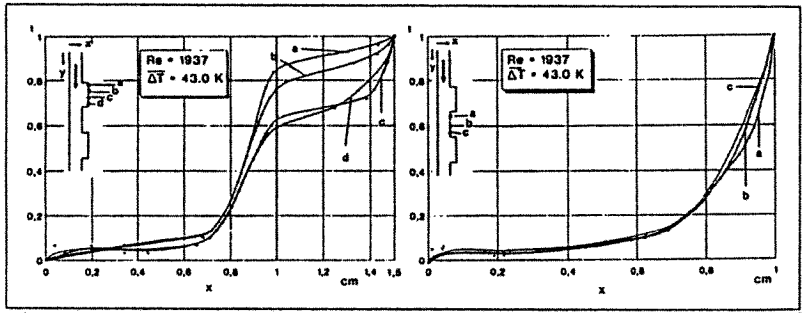

Fig. 6 Typical reconstructed temperature profiles at cross sections a) y = 5.18 cm, b) y = 6.16 cm, c) y = 6.78 cm and d) y = 6.96 cm in the region of the first groove (diagram left) and at cross sections a) y = 7.22 cm, b) y = 7.79 cm and c) y = 8.41 cm between the first groove and the second groove (diagram right) for Re = 1937 and $\overline{\Delta T}$ = 43 K.

In Fig. 4, for the forced convection situation, two main heat transfer regions can be recognized: (i) the main channel region and (ii) the region of the grooves. In the region of the grooves, temperature profiles are under the influence of the recirculating flow. Broad widely spaced fringes can be observed. There is no significant influence of recirculation in the channel part of the flow, and the temperature drop in this region is relatively high compared with the temperature drop in the groove (which can be seen from the temperature profiles). Downstream of the groove, along the heated wall, the fringe density increases, indicating high heat transfer coefficients. The decreasing thickness of the thermal boundary layer along the test section with increasing Reynolds numbers is clearly observable in the three forced convection interferograms. The temperature gradients at the heated channel wall increase with the increase in Reynolds number, which is similar to the situation in thermally developing duct flow with asymmetrical heating. The temperature gradient decreases in the channel region along the test section. At intermediate and higher Reynolds numbers (above Re = 600) a wide region of almost uniform temperature exists along the plane wall — the temperature corresponds approximately to the inlet air temperature or to the temperature of the plane wall. The visualized temperature fields agree qualitatively with the results obtained by numerical simulations [6-11].

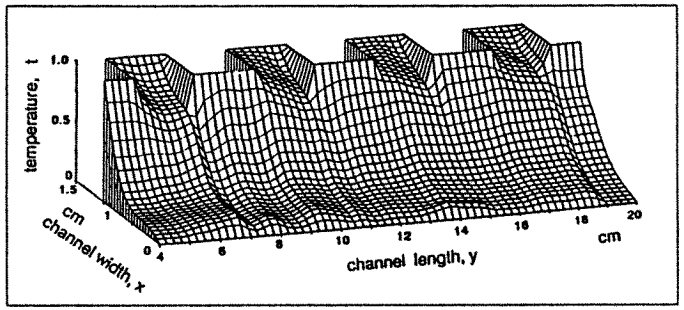

Fig. 7 Alternative representation of temperature fields reconstructed from interferograms at Re = 620 and $\overline{\Delta T}$ = 43.8 K. Flow direction is from left to right.

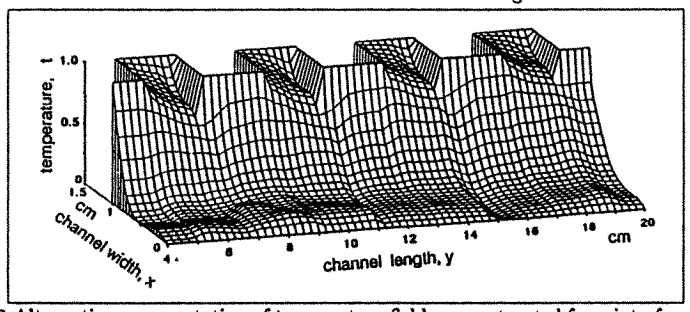

Fig. 8 Alternative representation of temperature fields reconstructed from interferograms at Re = 1481 and $\overline{\Delta T}$ = 43 K. Flow direction is from left to right.

The interferograms were evaluated by measuring locations of fringe minima and maxima at individual cross sections of the test channel using a photometer. The evaluation procedure which was described in [17] was used. Figures 5 and 6 show temperature profiles evaluated from the interferograms at individual channel cross sections in the groove region

and in the main channel region for the low Reynolds number situation (Re = 620) and for the high Reynolds number (Re = 1937) situation. The evaluated temperatures were scaled by $\overline{\Delta T}$ in order to obtain comparable results for the different experimental runs by different values of $T_C = T_{in}$ in the three channel heights.

In Figs. 5 and 6. left, temperature profiles at four different cross sections in the region of the first groove are presented. The temperature profiles show a characteristic S shape, similar to the results for a single cavity discussed by Aung [6]. The temperature gradient at the heated wall is small near the beginning of the groove, it increases along the groove to reach a maximum between the midpoint of the groove floor and the downstream wall, and then it decreases towards the downstream wall of the groove. In the main channel region, the temperature falls gradually for Re = 620 and abruptly for Re = 1937, to reach finally to the temperature of the plane wall. Figures 5 and 6 right, show temperature profiles in the region between the first and the second grooves, in the zone of the redeveloping thermal boundary sublayer. The temperature gradient is high immediately downstream of the first groove, and it gradually decreases towards the second groove. The temperature gradients at the heated wall are significantly higher for Re = 1937. For the following grooves and the channel regions between the grooves, the temperature profiles are similar.

In order to gain a better overall understanding of the temperature distribution, an alternative three dimensional representation was selected (Figs. 7 and 8). The values of the temperature in the mesh points were obtained by interpolation between discrete values obtained in the evaluation of interferometric fringes in the individual cross sections of the channel. An inspection of the temperature fields shows higher temperature gradients at the heated channel wall and also at the downstream wall of the groove for the higher Reynolds number situation in Fig. 8.

The temperature values obtained from interferometric measurements were compared with thermocouple readings, and the errors connected with the evaluation of temperature profiles were usually below 3%, only in exceptional cases the deviation reached up to 7%. More details about the accuracy of the reconstruction of temperature profiles from interferograms are given in [18].

Nusselt Numbers

In Fig. 9 , local Nusselt numbers Nu(y) along the heated wall (only on the vertical sections) together with the mean Nusselt numbers $\overline{Nu}_p$ for the three channel-groove periods visible in the interferograms, for Reynolds numbers of 620, 1076, 1481 and 1937 are presented. These results were obtained by averaging values from three experimental runs, while in earlier reports [2 and 3] the local Nusselt numbers were evaluated from a single experimental run. Also the mean Nusselt number for the thermally fully developed flow situation for the basic geometry, the assymetrically heated parallel plate channel, $\overline{Nu}_0$ which is 4 [5], is indicated in the figure, and it can serve as reference value in the analysis of heat transfer augmentation. The local Nusselt number is evaluated as

$$Nu(y) = \frac{(dT/dx)_w \, D_h}{(T_w - T_b)}, \tag{2}$$

where $(dT/dx)_w$ is the temperature gradient at the grooved wall and the bulk temperature T_b was taken as reference temperature. As the temperature of the cold wall corresponds to the ambient temperature as well as to the temperature of the air streaming along this wall.

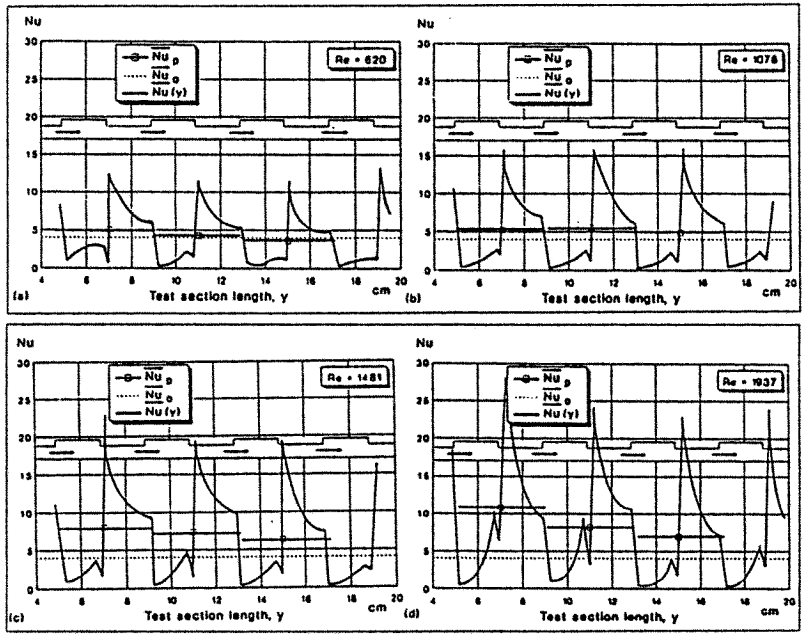

Fig. 9 Local Nusselt number Nu(y) along the test section, mean Nusselt number over channel-groove periods $\overline{Nu}_p$, and mean Nusselt number for the thermally fully developed situation for the asymmetrically heated parallel plate duct $\overline{Nu}_0$ for a) Re = 620, b) Re = 1076, c) Re = 1481 and d) Re = 1937.

local Nusselt numbers were not evaluated for the cold wall. The mean Nusselt number for a groove-channel period $\overline{Nu}_p$ is evaluated as

$$\overline{Nu}_p = \frac{\int_{period} Nu(y)dy}{\Delta y_p}. \tag{3}$$

The integration is performed along the groove-channel periods, the first period begins with the first groove (y = 5 cm) and ends at the end of the channel region (y = 9 cm) before the second groove, the second period begins at the beginning of the second groove (y = 9 cm) and so on (also indicated in the diagrams). The length of the period Δy_p is always 4 cm.

For all four flow velocities, the local Nusselt numbers show the same characteristic behaviour. Immediately at the beginning of the first goove they abruptly fall to a fraction of the attached flow value upstream of the groove. Along the groove they increase gradually, reaching a maximum between the midpoint of the groove and the downstream wall. After this maximum, the value of Nu(y) drops abruptly at y locations near the downstream wall. Nu(y) values in the groove are lower than in the channel, due to the low velocities in this

region [9]. At y locations in the channel region immediately downstream of the groove, Nu(y) reaches a new peak (region of the redeveloping thermal sublayer) — a multiple of the maximum value in the region of the groove. This peak is followed by a gradual decrease of Nu(y) in the streamwise direction towards the next groove. The behaviour of Nu(y) described above repeats along the test section for the following groove/channel sections.

Comparing the diagrams for the different Reynolds numbers, the absolute values of the peaks both in the grooves and in the inter-groove regions are higher for higher Reynolds numbers. At lower Reynolds numbers a nearly periodical trend is observable, while at higher Reynolds numbers the intensities of the maxima gradually decrease with increasing y coordinate. This behaviour can also be recognized in the interferograms presented in Fig. 4.

The average Nusselt numbers along the three groove-channel periods $\overline{Nu}_p$ decrease along the channel (except for a small increase in the second period at Re = 1076 where the values of $\overline{Nu}_p$ are very close), which can be explained by the thermally developing flow situation. The absolute values of $\overline{Nu}_p$ increase with increasing Reynolds numbers, and for the analysed four states they exceed the value of $\overline{Nu}_0$ for the three analized Reynolds numbers above 620.

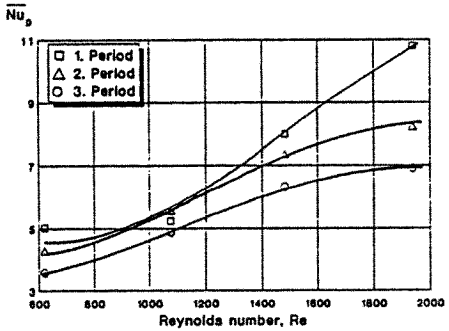

Fig. 10 Variation of the period average Nusselt number $\overline{Nu}_p$ with the Reynolds number for the three investigated groove-channel periods

Figure 10 shows the dependence of the period average Nusselt number $\overline{Nu}_p$ for the three investigated groove-channel periods as function of the Reynolds number: The values obtained for the four states in Fig 9. are entered into the plot. The decrease of the slope with the increasing y distance along the test section can be observed.

The local Nusselt numbers obtained experimentally, agree well with the results of the numerical investigations of Trollheden and Sundén [10], which were obtained for slightly different values of the Reynolds number and for the thermally fully developed regime. The local Nusselt numbers were evaluated from the temperature gradient on the heated wall, and the maximum deviations for the different experimental runs are around 10%. The accuracy of the evaluation of the Nusselt numbers can be increased by using automatic fringe analysis by means of digital image processing.

In Fig. 11, the variation of the overall Nusselt number $\overline{Nu}$, evaluated from the outlet-inlet temperature difference, is presented as function of the Reynolds number. The overall

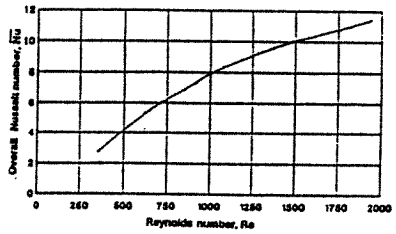

Fig. 11 Overall Nusselt number versus Reynolds number

Nusselt number was evaluated using the average heat transfer coefficient $\overline{\alpha}_H$ on the grooved wall

$$\overline{Nu} = \frac{\overline{\alpha}_H \, D_h}{k}. \tag{4}$$

$\overline{\alpha}_H$ is evaluated as

$$\overline{\alpha}_H = \frac{\dot{m} c_p}{A_H} \frac{T_{out} - T_{in}}{T_H - T_b} \tag{5}$$

with A_H as the heat transfer area of the hot wall. The overall Nusselt number $\overline{Nu}$ increases monotonuously with the increase of the Reynolds number. When compared with $\overline{Nu}_0$, an enhancement is achieved for Re > 450.

By introducing grooves into the basic geometry, the pressure drop increases up to a factor of 6.5. It increases with increasing Reynolds number. More details on the pressure drop measurements are presented in [4].

Conclusions

The experimental results presented in this paper indicate that enhancement of heat transfer in the grooved geometry is achieved, due to the periodical redevelopment of the thermal boundary layer in the region behind the grooves. Heat transfer in the main channel region is essentially uninfluenced by the recirculation in the groove and it contributes the most significant part to the total heat transfer. In the region of the grooves, the heat transfer is under the influence of the recirculating flow, and the temperature gradients at the heated wall are small. Temperature profiles show a characteristic S shape. For higher flow velocities the heat transfer is characterized by higher values of the local Nusselt number along the test section. The value of the mean Nusselt number for a groove-channel period $\overline{Nu}_p$ decreases along the channel due to the thermally developing flow. The values in the third groove-channel period are above the value $\overline{Nu}_0$, the mean Nusselt number for the hydrodynamically and thermally fully developed flow in an asymmetrically heated parallel plate channel, for three of the four investigated states for Re > 620. Increased heat transfer is accompanied by higher pressure drops — compared to the geometry with a smooth parallel flat plate channel — due to the increased skin friction in the redeveloping boundary layer and the existence of recirculating flow regions in the groove.

Future research should be concentrated on the comparison of experimental data and numerical results, in order to obtain sufficient information to predict system behaviour. A systematic analysis of the influence of groove dimensions and of the length of the region between the grooves on the heat transfer would provide valuable data for design purposes.

Nomenclature

A	heat transfer area, m^2
c_p	specific heat at constant pressure, J/kgK
d	width of the experimental channel, m
D_h	hydraulic diameter, $D_h = 4\ (2h\ d)\ /\ 2\ (2h + d)$, m
h	groove depth and one half of channel height, m
k	thermal conductivity, W/mK
Nu	Nusselt number, $Nu = \alpha D_h/k$
Δp	pressure drop between entry and exit of the test section, N/m^2
Re	Reynolds number, $Re = v_m D_h/\nu$
T	temperature, K
T_b	fluid bulk temperature, $T_b = (T_{in} + T_{out})/2$, K
$\overline{\Delta T}$	average temperature difference between hot wall and cold wall, K
t	scaled temperature, $t = (T(x) - T_C)\ /\ (T_H - T_C)$
v_m	cross channel average flow velocity, m/s
w	width of the grooves and of the inter-groove region, m
x	axis of the cartesian coordinate system across the channel, m
y	axis of the cartesian coordinate system in streamwise direction, m
z	axis of the cartesian coordinate system in spanwise direction, m
α	heat transfer coefficient, W/m^2K
λ	wavelength of laser light, m
ν	kinematic viscosity, m^2/s

Subscripts

0	basic geometry, parallel plate channel
b	mean
C	cold wall
H	hot wall
in	channel inlet
out	channel outlet
p	period average
w	wall

References

1. **Bergles, A. E.,** Techniques to augment heat transfer, in Handbook of heat transfer applications, eds. Rohsenow, W. M., Hartnett, J. P., Ganić, E. N., McGraw-Hill, NY, (1985).
2. **Webb, R. L.,** Enhancement of single-phase heat transfer, in Handbook of single-phase convective heat transfer, eds. Kakaç, S., Shah, R. K., Aung, W., John Wiley, NY, (1987).

3. **Herman, C. V., Mayinger, F.,** Experimental investigation of the heat transfer in laminar forced convection flow in a grooved channel, Proc. 9 Int. Heat Transfer Conference, Jerusalem, Israel, Vol.3, pp. 387-392, (1990).
4. **Herman, C. V., Mayinger, F.,** Interferometric study of heat transfer in a grooved geometry, paper accepted for the Second World Conference on Experimental Heat Transfer, Fluid Mechanics and Thermodynamics, Dubrovnik, Yugoslavia, June (1991).
5. **Shah, R. K., London, A. L.,** Laminar flow forced convection in ducts, in Advances in Heat Transfer, T. F. Irvine and J. P. Hartnett eds., Suppl. 1, (1978).
6. **Aung, W.,** An interferometric investigation of separated forced convection in laminar flow past cavities, ASME J. Heat Transfer, Vol. 106, pp. 505-512, (1983).
7. **Ghaddar, N. K., Korczak, K. Z., Mikić, B. B., Patera, A. T.,** Numerical investigation of incompressible flow in grooved channels. Part 1. Stability and self-sustained oscillations, J. Fluid Mech., Vol. 163, pp. 99- 127, (1986).
8. **Ghaddar, N. K., Magen, M., Mikić, B. B., Patera, A. T.,** Numerical investigation of incompressible flow in grooved channels. Part 2. Resonance and oscillatory heat transfer enhancement, J. Fluid Mech., Vol. 168, pp. 541-567, (1986).
9. **Amon, C. H., Mikić, B. B.,** Flow pattern and heat transfer enhancement in self-susteined oscillatory flows, paper AAIA - 89-0428 27th Aerospace Science Meeting, Reno, Nevada, (1989).
10. **Patera, A. T., Mikić, B. B.,** Exploiting heat transfer instabilities. Resonant heat transfer enhancement, Int. J. Heat Mass Transfer, Vol. 29, No. 8, pp. 1127-1138, (1986).
11. **Trollheden, S., Sundén, B.,** Numerical prediction of flow and heat transfer in a parallel duct with sreamwise periodic variation of cross- sectional area, Proc. 5 Int. Conf. on Numerical Methods in Laminar and Turbulent Flow, Montreal, Canada, Vol.5, Part 2, pp. 1515-1528, (1987).
12. **Sundén, B., Trollheden, S.,** Periodic laminar flow and heat transfer in a corrugated two-dimensional channel, Int. Comm. Heat Mass Transfer, Vol. 16, pp. 215-225, (1989).
13. **Lockett, J. F., Collins, M., W.,** Holographic interferometry applied to rib-roughness heat transfer in turbulent flow, Int. J. Heat Mass Transfer, Vol. 33, No. 11, pp. 2439-2449, (1990).
14. **Mayinger, F., Panknin, W.,** Holography in heat and mass transfer, Proc. 5 Int. Heat Transfer Conf., Tokyo, Japan, pp. 28-43, (1974).
15. **Vest, C. M.,** Holographic interferometry, John Wiley & Sons, New York, (1979).
16. **Herman, C. V., Mewes, D., Mayinger, F.,** Optical techniques in transport phenomena, to be published in Advances in Transport Processes VIII, A. S. Mujumdar, R. A. Mashelkar, eds., (1990).
17. **Hauf, W., Grigull, U.,** Optical methods in heat transfer, in Advances in Heat Transfer, Vol. 6, Academic Press Inc., New York, (1970).
18. **Sterr, S.,** Diplomarbeit, Lehrstuhl A für Thermodynamik, TU München, (1989).